Modeling Motor Responses of Paraplegics under Epidural Spinal Cord Stimulation: Computational Modeling Technical Report

Ellen R. Feldman and Joel W. Burdick*

1 Introduction

This technical report describes the computational model in our paper, *Modeling Motor Responses of Paraplegic Patients under Epidural Spinal Cord Stimulation*, appearing at the 2017 IEEE EMBS Conference on Neural Engineering. This model is the basis of our human spinal cord simulations.

The study utilizes the finite element method [1] to simulate the electrical activity within the spinal cord and nearby tissues; this technique numerically solves a system of partial differential equations over a specified geometry. Simulations were performed via COMSOL Multiphysics®, version 5.1. The following sections detail our modeling procedure, including the spinal cord geometry, equations solved over this domain, material properties, and finite element analysis.

2 Volume Conductor Model

The modeled geometry—also called the *volume conductor*—includes the spinal cord and surrounding biological tissues, as well as the Medtronic Specify$^{\text{TM}}$ 5-6-5 electrode array, implanted within the layer of epidural fat between the spinal cord and vertebrae. When stimulation is applied, electric current flows from the anodes (positive electrodes) to the cathodes (negative electrodes), resulting in a voltage distribution throughout the nearby tissues.

Our model, depicted in Figure 1, has a geometry largely based upon that of Ladenbauer (2008) [2]. It is comprised of gray matter, white matter, cerebrospinal fluid (CSF), dura mater, epidural fat, vertebral bone, intervertebral discs, ligaments, a thoracic/abdominal compartment, skin, and subcutaneous fat. Because the effects of the stimulation are concentrated close to the epidural array, we approximate the volume conductor's boundary as a rectangular prism.

The dura mater is modeled via a contact impedance boundary condition between the CSF and epidural fat; this condition approximates the dura as a thin layer of resistive material, via the following pair of equations:

$$\vec{n} \cdot \vec{J_1} = \frac{\sigma}{d_s}(V_1 - V_2) \tag{1}$$

$$\vec{n} \cdot \vec{J_2} = \frac{\sigma}{d_s}(V_1 - V_2), \tag{2}$$

where σ is the conductivity of the thin layer, d_s is its thickness, indices 1 and 2 refer to the two sides of the boundary, V is voltage, $\vec{J}$ is current density, and $\vec{n}$ is a unit vector normal to the boundary, pointing from side 1 toward side 2. These relations are derived via a first-order approximation of Ohm's Law, $\vec{J} = \sigma\vec{E} = -\sigma\nabla V$.

*E. Feldman and J. Burdick are with the Division of Engineering and Applied Science at the California Institute of Technology, Pasadena, CA 91125, USA {efeldman,jburdick}@caltech.edu

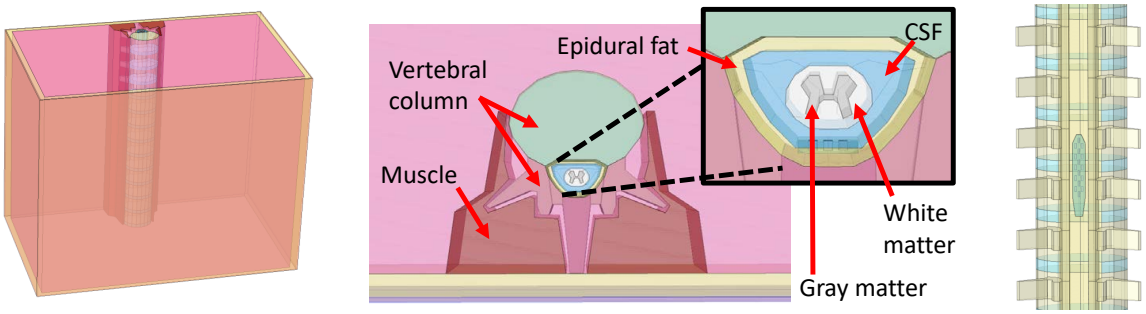

(a) (b) (c)

Figure 1: Volume conductor model. a) Side view. b) Top view. c) Vertebral column, with electrode array inside the epidural fat.

3 Equations Solved over the Volume Conductor

Similarly to studies by Ladenbauer and Capogrosso [2, 3], our finite element simulations solve Laplace's equation over the volume conductor:

$$\nabla \cdot (\sigma \nabla V) = 0, \tag{3}$$

where V is the electric potential and σ is the material's conductivity. We now show how to derive Laplace's equation, denoting $\vec{E}$ as the electric field, $\vec{J}$ as the current density, and ρ as the electric charge density.

We begin with the following relations from the theory of electromagnetics:

$$\vec{E} = -\nabla V \text{ (Definition of electric potential)} \tag{4}$$

$$\vec{J} = \sigma \vec{E} \text{ (Ohm's Law)} \tag{5}$$

$$\nabla \cdot \vec{J} = -\frac{\partial \rho}{\partial t} \text{ (Conservation of electric current).} \tag{6}$$

Substituting (4) into (5) and then (5) into (6) yields Poisson's equation:

$$\nabla \cdot (\sigma \nabla V) = \frac{\partial \rho}{\partial t}. \tag{7}$$

Obtaining Laplace's equation (3) from Poisson's equation (7) requires the quasistatic approximation, $\frac{\partial \rho}{\partial t} \approx 0$. This approximation assumes that charge density does not vary with time, or equivalently, that there is no charge build-up due to capacitive elements in the human body. Schwan and Kay [4] experimentally demonstrated that the ratio of capacitive to resistive currents in bodily tissue is negligible at frequencies below 1 kHz, validating the quasistatic approximation for frequencies in the 25-40 Hz range used in our experiment. Thus, our simulations consider the effect of each electrical stimulus only at the peak of the stimulation waveform, invoking the quasistatic approximation to neglect charge build-up caused by temporal variations.

Two types of boundary conditions are applied to the volume conductor. Dirichlet boundary conditions are applied to set electrodes to their desired potentials:

$$V(x) = V_0(\vec{x}),\ \vec{x} \in \Gamma_D, \tag{8}$$

where Γ_D is the set of all points located upon electrode surfaces. Secondly, the following Neumann boundary condition ensures that current is not permitted to flow outside of the volume conductor:

$$\vec{J}(\vec{x}) \cdot \vec{n} = (-\sigma \nabla V(\vec{x})) \cdot \vec{n} = \vec{0},\ \vec{x} \in \Gamma_N, \tag{9}$$

where Γ_N is the set of all points which lie upon the volume conductor's outer boundary.

4 Material Properties

In order to solve equation (3), electrical conductivities must be specified for all materials appearing in the model; Table 1 lists the values used in our study. All conductivities are modeled as isotropic except for the paraspinal muscles and white matter, for which the conductivities differ in the transverse and longitudinal directions.

With the exceptions of the general thoracic/abdominal cavity, as well as the materials comprising the electrode implant, these properties were drawn from Gabriel's 1996 study [5] and calculated at a frequency of 40Hz using 4-Cole-Cole regression models [5, 6]. It should be noted that in the two cases of skin and longitudinal muscle, we utilize the nearest data point in Gabriel's dataset rather than the 4-Cole-Cole predictions, since in these particular cases, the fits are less accurate (see [5]). Meanwhile, the value for the abdominal/thoracic compartment is drawn from Ladenbauer (2008) [2].

All materials listed are bodily tissues except for the components of the implant: a silicone rubber base and electrodes made from medical grade stainless steel, type 316. A very thin layer of platinum-iridium (Pt-Ir) is deposited upon the electrode surfaces, which we neglect in our model. The electrical conductivity for the stainless steel is drawn from the CRC Materials Science and Engineering Handbook [7], while for the silicone rubber, the conductivity comes from the AZoM online materials database [8].

Tissue/material	Conductivity (S/m)
Cerebrospinal fluid (CSF)	2.0
Dura mater	0.50
Fat (epidural)	0.019
Fat (subcutaneous)	0.019
Gray matter	0.068
General thoracic/abdominal cavity	0.25
Intervertebral discs	0.26
Ligaments	0.26
Muscle	0.23 transversally; 0.26 longitudinally
Skin	$18e^{-5}$
Vertebral bone	0.020
White matter	0.037 transversally; 0.097 longitudinally
Silicone	$3.3e^{-12}$
Stainless steel	$1.4e^{6}$

Table 1: Electrical conductivities of materials in the computational model.

Finally, although Gabriel only models the white matter as an isotropic material, white matter is known to be less conductive transversally than longitudinally, due to the presence of myelin [9]; this anisotropy can significantly impact simulation results. Therefore, we model the white matter using separate conductivities in the transverse and longitudinal directions. These values, obtained via the method discussed in De Geeter et al. (2012) [9], are determined by diffusion tensor imaging (DTI). Defining coordinate axes with $+x$ extending laterally to the right, $+y$ in the dorsal direction, and $+z$ in the caudal direction, the diffusion tensor is a diagonal matrix with elements d_{trans} corresponding to both transverse directions, and d_{long} corresponding to the z-direction. Letting σ_{iso} be the isotropic value for the conductivity, which we obtained from Gabriel (1996) [5], the relations described in Section 2.1 of De Geeter et al. [9] yield the following equations for the transversal conductivity σ_{trans} and longitudinal conductivity σ_{long}:

$$\sigma_{trans} = \sigma_{iso} * \frac{d_{trans}}{\sqrt[3]{d_{trans}^2 d_{long}}} \tag{10}$$

$$\sigma_{long} = \sigma_{iso} * \frac{d_{long}}{\sqrt[3]{d_{trans}^2 d_{long}}} \tag{11}$$

Using the water diffusion values for humans determined by Ellingson et al. (2008) [10], we obtain the anisotropic conductivity tensor for the white matter.

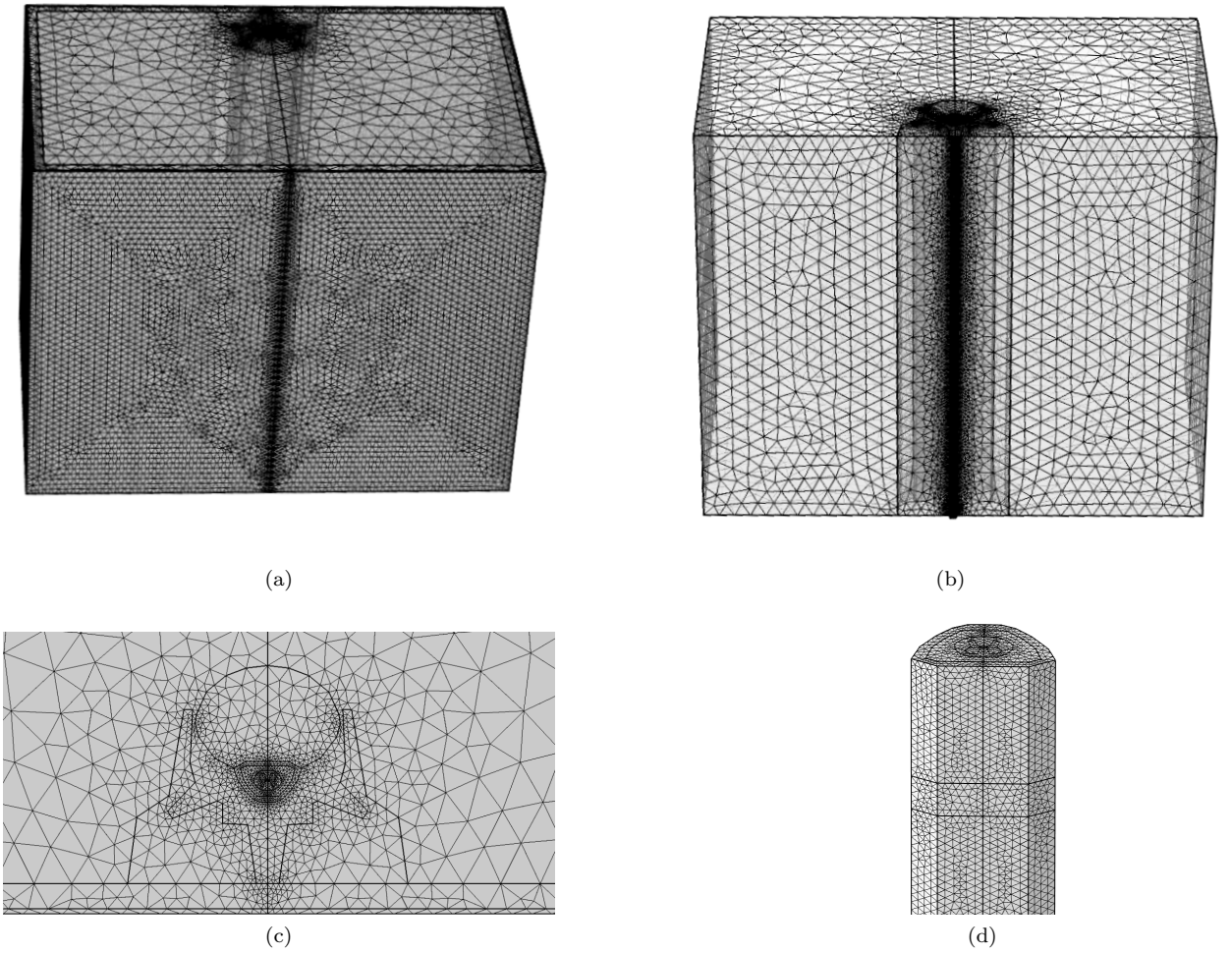

(a) (b)

(c) (d)

Figure 2: Finite element method mesh. a) Ventral view. b) Dorsal view, without outer skin and fat layers. c) Top view. d) Epidural fat, CSF, and spinal cord.

5 The Finite Element Method

Finite element meshing is performed via a Delaunay algorithm [11], which divides the volume conductor into tetrahedral elements over which partial differential equations may be approximated. This algorithm avoids small angles in element faces, and bounds the worst-case aspect ratio of the mesh elements [12]. As our geometry is symmetric across the coronal plane, we constrain the mesh to be symmetric across this plane. The mesh contains a total of 1,891,350 tetrahedral elements. Figure 2 displays several views of the mesh.

Utilizing the discrete tetrahedral elements produced by the Delaunay meshing algorithm, COMSOL Multiphysics® numerically solves Laplace's equation (3) and the two boundary conditions (8) and (9), discussed in Section 3, via finite element analysis [1]. COMSOL performs the finite element method using quadratic Lagrange shape functions together with the Galerkin method, that is, the same set of functions are used as both basis and test functions in performing the approximation; further details of COMSOL's approach may be found in COMSOL's Multiphysics Cyclopedia [13].

6 Acknowledgements

We are very grateful to Jeffrey Edlund for many extremely helpful conversations regarding the correct modeling of material properties. This work was supported by the National Science Foundation, the National Institutes of Health, and the Christopher and Dana Reeve Foundation.

References

[1] A. J. Davies, *The Finite Element Method: An Introduction with Partial Differential Equations*. OUP Oxford, Oxford, 2011.

[2] J. Ladenbauer, "Simulation of the excitation of human lower spinal cord structures with surface electrodes: 3D finite element analysis and nerve fiber modeling," Master's thesis, Vienna Univ. Techn., 2008.

[3] M. Capogrosso, N. Wenger, S. Raspopovic, P. Musienko, J. Beauparlant, L. B. Luciani, G. Courtine, and S. Micera, "A computational model for epidural electrical stimulation of spinal sensorimotor circuits," *J. Neuroscience*, vol. 33, no. 49, pp. 19326–19340, 2013.

[4] H. P. Schwan and C. F. Kay, "Capacitive properties of body tissues," *Circulation Research*, vol. 5, no. 4, pp. 439–443, 1957.

[5] C. Gabriel, "Compilation of the dielectric properties of body tissues at rf and microwave frequencies.," tech. rep., DTIC Document, 1996.

[6] C. Andreuccetti, R. Fossi, and C. Petrucci, "An Internet resource for the calculation of the dielectric properties of body tissues in the frequency range 10 Hz - 100 GHz." `http://niremf.ifac.cnr.it/tissprop/`. IFAC-CNR, Florence (Italy), 1997. Based on data published by C.Gabriel et al. in 1996.

[7] J. F. Shackelford and W. Alexander, *CRC materials science and engineering handbook*. CRC press, 2001.

[8] "Silicone rubber." AZO Materials. `http://www.azom.com/properties.aspx?ArticleID=920`. Accessed: 2017-02-16.

[9] N. De Geeter, G. Crevecoeur, L. Dupré, W. Van Hecke, and A. Leemans, "A DTI-based model for TMS using the independent impedance method with frequency-dependent tissue parameters," *Physics in medicine and biology*, vol. 57, no. 8, p. 2169, 2012.

[10] B. Ellingson, J. Ulmer, S. Kurpad, and B. Schmit, "Diffusion tensor MR imaging of the neurologically intact human spinal cord," *American Journal of Neuroradiology*, vol. 29, no. 7, pp. 1279–1284, 2008.

[11] R. Dyer, H. Zhang, and T. Möller, "Delaunay mesh construction," in *Symposium on geometry processing*, pp. 273–282, 2007.

[12] L. P. Chew, "Guaranteed-quality delaunay meshing in 3D (short version)," in *Proceedings of the thirteenth annual symposium on Computational geometry*, pp. 391–393, ACM, 1997.

[13] "The finite element method (FEM)." COMSOL Multiphysics Cyclopedia. `https://www.comsol.com/multiphysics/finite-element-method`. Accessed: 2017-03-23.